The long egress of GJ 436b's giant exosphere

B. Lavie, D. Ehrenreich, V. Bourrier, A. Lecavelier Des Etangs, A. Vidal-Madjar, X. Delfosse, A. Gracia Berna, K. Heng, N. Thomas, S. Udry, et al.

▶ **To cite this version:**

B. Lavie, D. Ehrenreich, V. Bourrier, A. Lecavelier Des Etangs, A. Vidal-Madjar, et al.. The long egress of GJ 436b's giant exosphere. Astronomy & Astrophysics - A&A, 2017, 605, 10.1051/0004-6361/201731340 . insu-03692485

HAL Id: insu-03692485
https://insu.hal.science/insu-03692485v1

Submitted on 10 Jun 2022

HAL is a multi-disciplinary open access archive for the deposit and dissemination of scientific research documents, whether they are published or not. The documents may come from teaching and research institutions in France or abroad, or from public or private research centers.

L'archive ouverte pluridisciplinaire **HAL**, est destinée au dépôt et à la diffusion de documents scientifiques de niveau recherche, publiés ou non, émanant des établissements d'enseignement et de recherche français ou étrangers, des laboratoires publics ou privés.

A&A 605, L7 (2017)
DOI: 10.1051/0004-6361/201731340
© ESO 2017

Astronomy & Astrophysics

Letter to the Editor

The long egress of GJ 436b's giant exosphere

B. Lavie[1,2], D. Ehrenreich[1], V. Bourrier[1], A. Lecavelier des Etangs[3], A. Vidal-Madjar[3], X. Delfosse[5], A. Gracia Berna[2], K. Heng[2], N. Thomas[2], S. Udry[1], and P. J. Wheatley[4]

[1] Observatoire de l'Université de Genève, 51 chemin des Maillettes, 1290 Sauverny, Switzerland
e-mail: baptiste.lavie@unige.ch
[2] University of Bern, Space Research and Planetary Sciences, Sidlerstrasse 5, 3012 Bern, Switzerland
[3] CNRS, Institut d'Astrophysique de Paris, UMR 7095, 98bis boulevard Arago, 75014 Paris, France
[4] Dept. of Physics, University of Warwick, Gibbet Hill Road, Coventry CV4 7AL, UK
[5] Univ. Grenoble Alpes, CNRS, IPAG, 38000 Grenoble, France

Received 9 June 2017 / Accepted 19 August 2017

ABSTRACT

The M dwarf GJ 436 hosts a transiting warm Neptune known to experience atmospheric escape. Previous observations revealed the presence of a giant hydrogen exosphere transiting the star for more than 5 h, and absorbing up to 56% of the flux in the blue wing of the stellar Lyman-α line of neutral hydrogen (H I Lyα). The unexpected size of this comet-like exosphere prevented observing the full transit of its tail. In this Letter, we present new Lyα observations of GJ 436 obtained with the Space Telescope Imaging Spectrograph (STIS) instrument onboard the *Hubble* Space Telescope. The stability of the Lyα line over six years allowed us to combine these new observations with archival data sets, substantially expanding the coverage of the exospheric transit. Hydrogen atoms in the tail of the exospheric cloud keep occulting the star for 10–25 h after the transit of the planet, remarkably confirming a previous prediction based on 3D numerical simulations with the EVaporating Exoplanet code (EVE). This result strengthens the interpretation that the exosphere of GJ 436b is shaped by both radiative braking and charge exchanges with the stellar wind. We further report flux decreases of 15 ± 2% and 47 ± 10% in the red wing of the Lyα line and in the line of ionised silicon (Si III). Despite some temporal variability possibly linked with stellar activity, these two signals occur during the exospheric transit and could be of planetary origin. Follow-up observations will be required to assess the possibility that the redshifted Lyα and Si III absorption signatures arise from interactions between the exospheric flow and the magnetic field of the star.

Key words. planets and satellites: atmospheres – planets and satellites: gaseous planets – planets and satellites: individual: GJ 436

1. Introduction

Transit observations in the stellar Lyman-α line of neutral hydrogen (H I Lyα at 1215.67 Å) allowed the detection of atmospheric escape from the two hot Jupiters HD 209458b (Vidal-Madjar et al. 2003, 2004) and HD 189733b (Lecavelier des Etangs et al. 2010, 2012; Bourrier et al. 2013), the warm giant 55 Cnc b (Ehrenreich et al. 2012), and the warm Neptune GJ 436b (Kulow et al. 2014; Ehrenreich et al. 2015). The escaping hydrogen exospheres produce large Lyα absorption transit signatures ranging from 7.5 ± 1.8% for 55 Cnc b to 56.3 ± 3.5% for GJ 436b. Compared to close-in hot Jupiters, GJ 436b (25.4 ± 2.1 $M_\oplus$ and 4.10 ± 0.16 $R_\oplus$, Butler et al. 2004; Gillon et al. 2007; Lanotte et al. 2014) is gently irradiated by its M2V host star (Ehrenreich et al. 2011), yet it spots an extended hydrogen envelope, first hinted at by Kulow et al. (2014) and fully revealed by Ehrenreich et al. (2015). These authors found that GJ 436b emits a comet-like cloud of H atoms, with a coma bigger than the star and a tail extending millions of kilometers (up to 40% of GJ 436b's orbit, 450 planetary radii), trailing the planet. Because of its unexpected, gigantic scale, past Lyα observations of GJ 436b's exosphere could only cover the transit of its coma and the onset of its comet-like tail. Bourrier et al. (2015, 2016b) have modelled the dynamics of GJ 436b exospheric cloud using the EVaporating Exoplanets code (`EVE`; Bourrier & Lecavelier des Etangs 2013). Adjusting Lyα spectra obtained between 2010 and 2014, they show that the geometry and dynamical structure of the exospheric cloud could be explained by radiative braking (i.e. the effect on exosphere particles resulting from radiation pressure lower than stellar gravity; Bourrier et al. 2015) and stellar wind interaction (specifically, charge exchange; Bourrier et al. 2016b). The balance between both mechanisms, however, would shape the cloud tail, hence the egress of the UV transit, differently. Meanwhile, the full extent of the tail, provided by the egress duration, is unknown. Given the partial coverage (3–4h) of the egress, new data were needed to fully cover the UV transit egress and precisely determine the nature of the star-planet interaction sculpting the cloud.

In this Letter, we present new *Hubble* Space Telescope (HST) data obtained with the Space Telescope Imaging Spectrograph (STIS). The combined reduction and analysis of these data covering a much larger fraction of the planetary orbit, with all previously existing data, is presented in Sect. 3 and Appendix B. Our results (Sect. 4) confirm the blueshifted Lyα absorption signature of Ehrenreich et al. (2015) and strengthen the interpretation of Bourrier et al. (2015, 2016b). We also find new surprising absorption signatures in the red wing of the H I Lyα line and in the ionised silicon line (Si III) that could be of planetary or stellar origins.

2. Observations

In total, GJ 436b has been observed at eight epochs (hereafter Visits 0 to 7) with HST/STIS. All visits are listed in Table A.1. Visits 0 to 3 revealed the deep transit of GJ 436b's exosphere in the blue wing of the Lyα line (Ehrenreich et al. 2011, 2015; Kulow et al. 2014). Three new visits (Visits 5 to 7) were obtained

on 2016-Mar-30, 2016-Apr-06, and 2016-May-08 (General Observer (GO) programme 14222; PI: D. Ehrenreich) with the aim of completing the coverage of the exospheric transit, during the transit of the tail (~+3,+20 h; Visit 6), before the transit of the coma ($\lesssim$−3 h; Visit 7), and after the presumed end of the transit ($\gtrsim$+20 h; Visit 5). Times are calculated using the ephemeris from Lanotte et al. (2014). All observations were made with the Far Ultraviolet Multi-Anode Microchannel Array detector (FUV-MAMA) detector and the G140M grating with a central wavelength of 1222 Å. The eight visits represent 27 HST orbits. Each orbit-long[1] time-tag exposure has been divided into five sub-exposures (a reasonable balance between signal over noise ratio and time resolution) and processed through `CALSTIS`, the STIS pipeline, yielding a total of 135 spectra.

3. Analysis

3.1. Reference, unocculted Lyα flux

The new visits obtained before and after the exospheric transit allow us to reconstruct a reference spectrum seemingly unaffected by the exospheric absorption signature. We average the flux in the first HST orbits of Visits 0, 2, and 3 (as done by Ehrenreich et al. 2015) with the flux measured in all HST orbits obtained during Visits 4, 5, and 7. This average out-of-transit baseline spectrum appears stable in both the red wing of the Lyα line and the reference band ($[-250,-120] \cup [+120,+250]$ km s^{-1}), as can be seen in Fig. 1a,b. In the Lyα blue wing (Fig. 2), the flux of Visit 4 and the first exposure of Visit 5 are higher than in subsequent orbits used for the out-of-transit baseline. The origin of this wavelength-dependent rise is unclear, but in the following we chose to include them in the out-of-transit baseline flux. Excluding them will only decrease the out-of-transit baseline by less than 4%.

3.2. Correction of systematics

In addition to stellar variability, STIS G140M spectra are known to be impacted by an instrumental systematic effect caused by the telescope breathing. This effect is reported to be achromatic, thus to correct for it we need to locate a reference wavelength or velocity band in the Lyα emission feature devoid of astrophysical signal. The geocoronal emission line (airglow) contaminates the core of the observed stellar line, and varies in strength and position from one observation to another. This region is not adapted to our needs so we exclude it, setting conservative limits of $[-40,+30]$ km s^{-1} (velocities are expressed with respect to the Lyα line centre in the stellar rest frame). Previous work reported absorption signatures in the Lyα blue wing ($[-120,-40]$ km s^{-1}; Ehrenreich et al. 2015) and, tentatively, in the Lyα red wing ($[+30,+120]$ km s^{-1}; Kulow et al. 2014). These two bands, over which we will search for exospheric signatures, cannot be used to monitor telescope breathing. A careful inspection of the Lyα spectra presented in Fig. 3 allowed us to find two bands seemingly free of astrophysical signal, over $[-250,-120]$ and $[+120,+250]$ km s^{-1}, which we call the reference band. The flux integrated over these two bands, which can be seen in Fig. A.1c, remains about stable within the uncertainties for all visits, spanning over six years of observations. We hypothesized that all variations in these reference bands could be attributed to instrumental effect. Different strategies have been developed to correct for telescope breathing (see e.g. Bourrier et al. 2017, and references therein). In this work, we compare three correction methods: parametric (Bourrier & Lecavelier des Etangs 2013; Ehrenreich et al. 2012; Bourrier et al. 2016a), empirical (Deming et al. 2013; Wilkins et al. 2014; Berta et al. 2012; Ehrenreich et al. 2014), and non-parametric using Gaussian processes (GP; Appendix B). All three methods yield similar results. In the following, we opt to rely on the GP-based approach.

[1] The exposure time ranges from ~1500 to 2900 s.

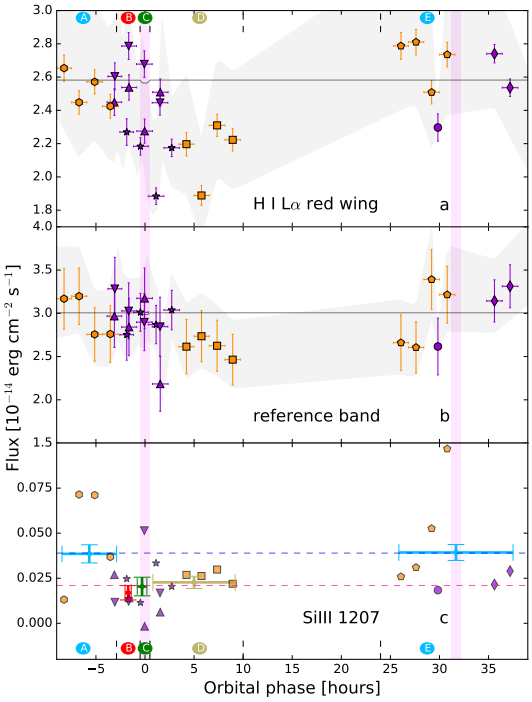

Fig. 1. Light curves of GJ 436 integrated Lyα red wing (*a*), Lyα reference band $[-250,-120] \cup [+120,+250]$ km s^{-1} (*b*) and Si III line (*c*). New visits described in this work are in orange while previous visits are plotted in violet. Symbols are in Table A.1. Different temporal regions are defined: (A) before transit, (B) ingress, (C) optical transit, (D) egress, and (E) after transit. The grey-filled region represents the 1σ confidence interval of the systematic correction method using the Gaussian processes (Appendix B). The vertical magenta zones show the optical primary and secondary transit. The optical transit light curve of GJ 436b is indicated with the black line. In *panel c*, fluxes are integrated for the different temporal region (see Fig. 2). Horizontal dashed lines indicate the out-of-transit flux (blue – regions A and E) and the in-transit flux (pink – regions B, C, and D).

3.3. Flux in other spectral lines

Besides the prominent Lyα line, we detect the following stellar emission features in the STIS/G140M range (1190–1250 Å): Si III at 1206.5 Å, N V doublet at 1238.8 and 1242.8 Å, and O V at 1218.3 Å (cf. Table C.1). The low signal-to-noise ratio in these lines prevented us from doing an orbit-to-orbit comparison and establishing the stability of the stellar baseline flux for those lines. We therefore averaged their spectra within the orbital phase regions labelled A to E in Fig. 2 (cf. Table A.2): (A) before the exospheric transit signature in the blue wing of Lyα, (B) during the exospheric transit ingress, (C) during the optical transit (i.e. the transit of the planetary disk alone), (D) during the exospheric transit egress, and (E) after the exospheric transit. Regions (B), (C), and (D) are considered "in transit"; regions (A) and (E) are "out of transit".

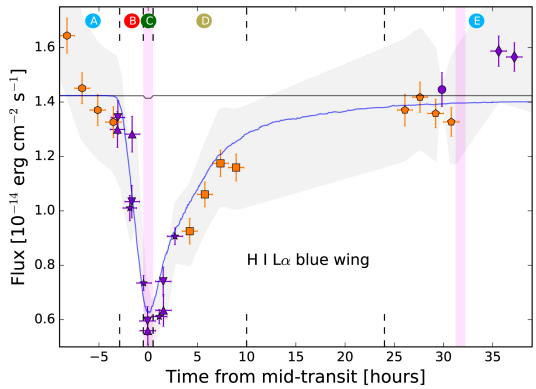

Fig. 2. Light curves of GJ 436 integrated over the Lyα blue wing. Legend is the same as in Fig. 1. The blue curve is the model calculated with EVE that represents the best fit to previous data (Visit 0 to 3).

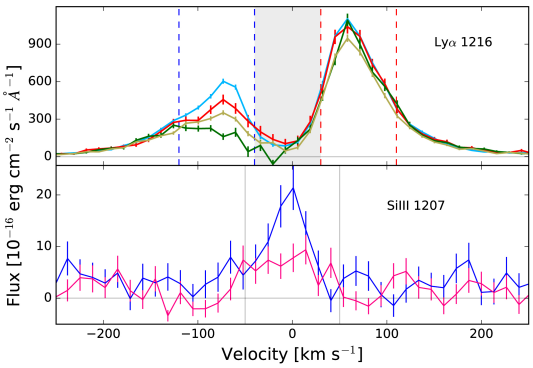

Fig. 3. *Top panel*: averaged out-of-transit (blue), ingress (red), egress (khaki), and in-transit (green) spectra of the Lyα line at 1206.5 Å. The grey zone is the geocoronal emission (airglow) band. *Bottom panel*: averaged out-of-transit (blue) and in-transit (pink) spectra of the Si III at 1206.5 Å. Vertical grey line indicates the $[-50, +50]$ km s^{-1} area.

4. Results

4.1. Detection of the Lyα transit egress

The most significant absorption signal is detected in the Lyα blue wing between −120 and −40 km s^{-1} (Fig. 2), in agreement with Ehrenreich et al. (2015). Visit 6 (time from mid-transit τ = [+4.01, +9.18] h) prolongates and confirms the exospheric egress suggested by Visits 1, 2, and 3. The egress duration is now constrained to be longer than ∼10 h and shorter than ∼25 h. The Lyα flux measured during Visit 5 (τ = [+25.8, +31.0] h) is in good agreement with the Visit 0 measurement obtained ∼+30 h after the mid-transit time, close to superior conjunction. We stress that those compatible measurements were obtained more than six years apart, highlighting the temporal stability of GJ 436. Bourrier et al. (2015, 2016a) fitted the spectra obtained during Visits 0 to 3 (all violet curves in Fig. A.2) with EVE. Their best-fit theoretical spectra yield the light curve plotted in Fig. 2. The model is in remarkable agreement with the new data from Visits 6 and 7, strengthening the interpretation proposed in Bourrier et al. (2015, 2016a): the weak UV radiation emitted by GJ 436 yields a low radiation pressure (∼70% of stellar gravity) and a low photoionisation of escaping hydrogen atoms. This, combined with a high planetary wind velocity (∼55 km s^{-1}), allows the planetary outflow to diffuse within a large coma surrounding and comoving with the planet, which further extends into a broad cometary tail (Bourrier et al. 2015). In addition, escaping atoms interact with the slow stellar wind of the M dwarf (∼85 km s^{-1}) via charge exchanges abrading the day-side exosphere (Bourrier et al. 2016a). These interactions create a secondary tail of neutralised stellar wind protons[2], which move with the persistent dynamics of the stellar wind and therefore yield different Lyα absorption signatures over time than the primary tail. This model assumed that the out-of-transit baseline is provided by the flux measured during the "out-of-transit" region defined in the previous section. Visits 4 and 7 tentatively suggest (Fig. 2), however, that the unocculted Lyα line might be even brighter. This will have to be confirmed with additional measurements obtained between the superior conjunction and the first quadrature.

4.2. Detection of a redshifted Lyα absorption signature

Visits 1 and 6 show similar integrated fluxes in the Lyα red wing during and after the optical transit, with an average absorption depth of 15 ± 2% compared to the baseline level (Figs. 1a and 3). In both visits, the absorption signature is located within $[+30, +110]$ km s^{-1} but at a different time from the mid-transit at +0.5 and +6.6 h, respectively. In comparison, the blueshifted absorption occurs around the mid-transit. This redshifted absorption is time variable. This was first noted by Kulow et al. (2014) from Visit 1 data; however, Ehrenreich et al. (2015) did not confirm it with same-phase data obtained during Visits 2 and 3. Visit 6 changes this picture and confirms the existence of a redshifted Lyα signature delayed in time with respect to the blueshifted signature. Interpretation of this redshifted Lyα signature is challenging: the EVE model that best fitted the blueshifted signature (Sect. 4.1) does predict the existence of H atoms moving towards the star, but redshifted by less than +50 km s^{-1} because this population is localised within the coma and could not create a signature in the tail (see Fig. 4 in Bourrier et al. 2016a). In the absence of radiation pressure or with a very strong self-shielding protecting the interior of the coma (which is not the case for GJ436b), Bourrier et al. (2015) showed that gravitational shear could lead to a stream of H atoms falling onto the star but ahead of the planet and thus yielding a redshifted signature before the optical transit (see their Fig. 2). Interestingly, tentative Lyα redshifted absorptions have been previously reported in HD 209458b and HD 189733b (Vidal-Madjar et al. 2003; Lecavelier des Etangs et al. 2012) but in phase with the respective blueshifted absorptions signature of those planets.

It is plausible that stellar variability (Tian et al. 2009; Llama & Shkolnik 2016; Vidal-Madjar 1975) is the origin of the variations, because they are located at the peak of the observed red wing, which traces higher altitudes in the chromosphere of the star which are more active than the lower chromosphere which is the source for the far wings of the Lyα line (e.g. Bourrier et al. 2017). However, the high stability of the stellar flux over six years of observations, the fact that the variations always correspond to a decrease of the flux with respect to the reference spectrum, and the fact that they appear to be phased during and after the planet transit, suggest another scenario.

Interaction of the exospheric flow with the star and planet magnetic fields could be one of the mechanisms that drives particles towards the star. A bow shock formed ahead of the planet by the interaction between the stellar wind and the planetary magnetosphere could only yield absorption before the planet transit (Alexander et al. 2016; Lai et al. 2010). Furthermore, Bourrier et al. (2016a) showed that the interactions between the

[2] These are stellar wind protons that gained an electron from the interaction with neutral hydrogen atoms in the exosphere.

exosphere and the stellar wind required to explain the absorption in the Lyα blue wing imply that the planetary magnetosphere is embedded deep inside the coma. Strong magnetic connection could nonetheless link the embedded magnetosphere with the stellar magnetic field, forcing part of the planetary outflow to stream toward the star behind the planet (Strugarek 2016). One of the magnetised star-planet interactions proposed by Matsakos et al. (2015) (Type 4) bears some resemblance with our observations in the red wing, with planetary gas infalling nearly radially onto the star. The variability of the detected absorption could be explained by the continuous readjustment of the magnetic field topology as the planet orbits the star, with new magnetic accretion channels forming periodically. However, this scenario requires a high UV irradiation and a weak planetary outflow, which are not consistent with the mild irradiation from GJ 436 and the high velocities derived for the planetary outflow (Bourrier et al. 2016a). Furthermore, Matsakos et al. (2015) investigated the case of a hot Jupiter around a solar-type star, without accounting for radiation pressure despite its major role in shaping the exospheres of evaporating exoplanets. Gas in magnetised interaction regions is also expected to be strongly ionised, which would require either that massive amounts of neutral hydrogen infall toward the star or that shielding or recombination mechanisms allow for a significant portion of this gas to remain neutral.

4.3. Detection of an absorption signature from ionised silicon

The other stellar lines (Table C.1) are much fainter than Lyα, so we compared for each line the total fluxes averaged in transit (phase regions B, C and D) and out of transit (phase regions A and E). We report an absorption signal of 36 ± 15% in the O V line. The signal occurs during ingress and egress but not during the optical transit. Thus, it may not be of planetary origin. Loyd et al. (2017) observed GJ 436 with HST/Cosmic Origins Spectrograph (COS) from [−4, +3] h around the optical transit. Within this time range, they reported no detection of N V or Si III absorption. This is in agreement with our analysis of the two N V lines. Meanwhile, we detect an absorption signal of 47 ± 10% in the Si III line within [−50, +50] km s^{-1}, similar in intensity to the blueshifted Lyα absorption depth and occuring during the same phases as the exospheric transit. The flux is constant over the phase range covered by Loyd et al. (2017) (Fig. 1 c), suggesting that the stellar line was already absorbed during their observations, preventing them from detecting any variations. We note that our observations are compatible with their upper limit. We cannot exclude stellar variations in the Si III line (Loyd et al. 2017), which could be linked to the variation seen in the Lyα red wing (Sect. 4.2). A planetary origin for the Si III signal is tantalising, as it would demonstrate the hydrodynamic nature of GJ 436b atmospheric escape, constrain the star-planet magnetic interaction, and provide a possible tracer for the presence of enstatite clouds ($Mg_2Si_2O_6$), potentially responsible for the flat near-infrared transmission spectrum of the lower atmosphere (Knutson et al. 2014). This will require additional observations.

5. Conclusion

We report new HST/STIS UV observations of the exospheric cloud escaping from the warm Neptune GJ 436b. A combined analysis of all available UV data, making use of GP to correct for systematics, yields the following results:

1. We detect the UV transit egress and constrain its duration between 10 to 25 h. This corresponds to a size of the exospheric hydrogen tail between 5 and 12 millions km. This result confirms previous observations (Ehrenreich et al. 2015) and their interpretation (Bourrier et al. 2015, 2016a).
2. We detect an absorption signal in the red wing of the Lyα line, which is delayed in time compared to the blueshifted absorption. This signal could originate either from the planet or be due to stellar activity.
3. We detect an absorption signal in the Si III line, possibly linked with the Lyα redshifted signal (and stellar activity). More observations will be needed at other phases to discriminate the stellar activity scenario from a planetary origin.
4. We notice the remarkable stability of GJ 436's unocculted Lyα emission line over the six-year period (2010–2016) covered by the available observations.

Acknowledgements. We thank the referee, Allison Youngblood, for useful and fruitful comments. This work is based on observations made with the NASA/ESA *Hubble* Space Telescope. This work has been carried out in the frame of the National Centre for Competence in Research "PlanetS" supported by the Swiss National Science Foundation (SNSF). B.L., D.E., V.B., K.H., N.T., and S.U. acknowledge the financial support of the SNSF. A.L. acknowledges financial support from the Centre National d'Études Spatiales (CNES). P.W. is supported by the UK Science and Technology Facilities Council under consolidated grant ST/P000495/1. The authors acknowledge the support of the French Agence Nationale de la Recherche (ANR), under programme ANR-12-BS05-0012 "Exo-Atmos". This project has received funding from the European Research Council (ERC) under the European Union's Horizon 2020 research and innovation programme (project Four Aces; grant agreement No. 724427).

References

Alexander, R. D., Wynn, G. A., Mohammed, H., Nichols, J. D., & Ercolano, B. 2016, MNRAS, 456, 2766
Ambikasaran, S., Foreman-Mackey, D., Greengard, L., Hogg, D. W., & O'Neil, M. 2014, ArXiv e-prints [arXiv:1403.6015]
Berta, Z. K., Charbonneau, D., Désert, J.-M., et al. 2012, ApJ, 747, 35
Bourrier, V., & Lecavelier des Etangs, A. 2013, A&A, 557, A124
Bourrier, V., Lecavelier des Etangs, A., Dupuy, H., et al. 2013, A&A, 551, A63
Bourrier, V., Ehrenreich, D., & Lecavelier des Etangs, A. 2015, A&A, 582, A65
Bourrier, V., Ehrenreich, D., King, G., et al. 2016a, A&A, 597, A26
Bourrier, V., Lecavelier des Etangs, A., Ehrenreich, D., Tanaka, Y. A., & Vidotto, A. A. 2016b, A&A, 591, A121
Bourrier, V., Ehrenreich, D., King, G., et al. 2017, A&A, 597, A26
Butler, R. P., Vogt, S. S., Marcy, G. W., et al. 2004, ApJ, 617, 580
Deming, D., Wilkins, A., McCullough, P., et al. 2013, ApJ, 774, 95
Ehrenreich, D., Lecavelier des Etangs, A., & Delfosse, X. 2011, A&A, 529, A80
Ehrenreich, D., Bourrier, V., Bonfils, X., et al. 2012, A&A, 547, A18
Ehrenreich, D., Bonfils, X., Lovis, C., et al. 2014, A&A, 570, A89
Ehrenreich, D., Bourrier, V., Wheatley, P. J., et al. 2015, Nature, 522, 459
Gibson, N. P., Aigrain, S., Roberts, S., et al. 2012, MNRAS, 419, 2683
Gillon, M., Pont, F., Demory, B.-O., et al. 2007, A&A, 472, L13
Knutson, H. A., Benneke, B., Deming, D., & Homeier, D. 2014, Nature, 505, 66
Kulow, J. R., France, K., Linsky, J., & Loyd, R. O. P. 2014, ApJ, 786, 132
Lai, D., Helling, C., & van den Heuvel, E. P. J. 2010, ApJ, 721, 923
Lanotte, A. A., Gillon, M., Demory, B.-O., et al. 2014, A&A, 572, A73
Lecavelier des Etangs, A., Ehrenreich, D., Vidal-Madjar, A., et al. 2010, A&A, 514, A72
Lecavelier des Etangs, A., Bourrier, V., Wheatley, P. J., et al. 2012, A&A, 543, L4
Llama, J., & Shkolnik, E. L. 2016, ApJ, 817, 81
Loyd, P. R. O., Koskinen, T. T., France, K., Schneider, C., & Redfield, S. 2017, ApJ, 834, L17
Matsakos, T., Uribe, A., & Königl, A. 2015, A&A, 578, A6
Strugarek, A. 2016, ApJ, 833, 140
Tian, H., Curdt, W., Marsch, E., & Schühle, U. 2009, A&A, 504, 239
Vidal-Madjar, A. 1975, Sol. Phys., 40, 69
Vidal-Madjar, A., Lecavelier des Etangs, A., Désert, J.-M., et al. 2003, Nature, 422, 143
Vidal-Madjar, A., Désert, J.-M., Lecavelier des Etangs, A., et al. 2004, ApJ, 604, L69
Wilkins, A. N., Deming, D., Madhusudhan, N., et al. 2014, ApJ, 783, 113
Williams, C. R. C. 2006, Gaussian Processes for Machine Learning (The MIT press)

Appendix A: Log of observations and raw light curves

All spectra were linearly interpolated on a common wavelength grid, chosen to be the grid of Visit 0 first sub-exposure.

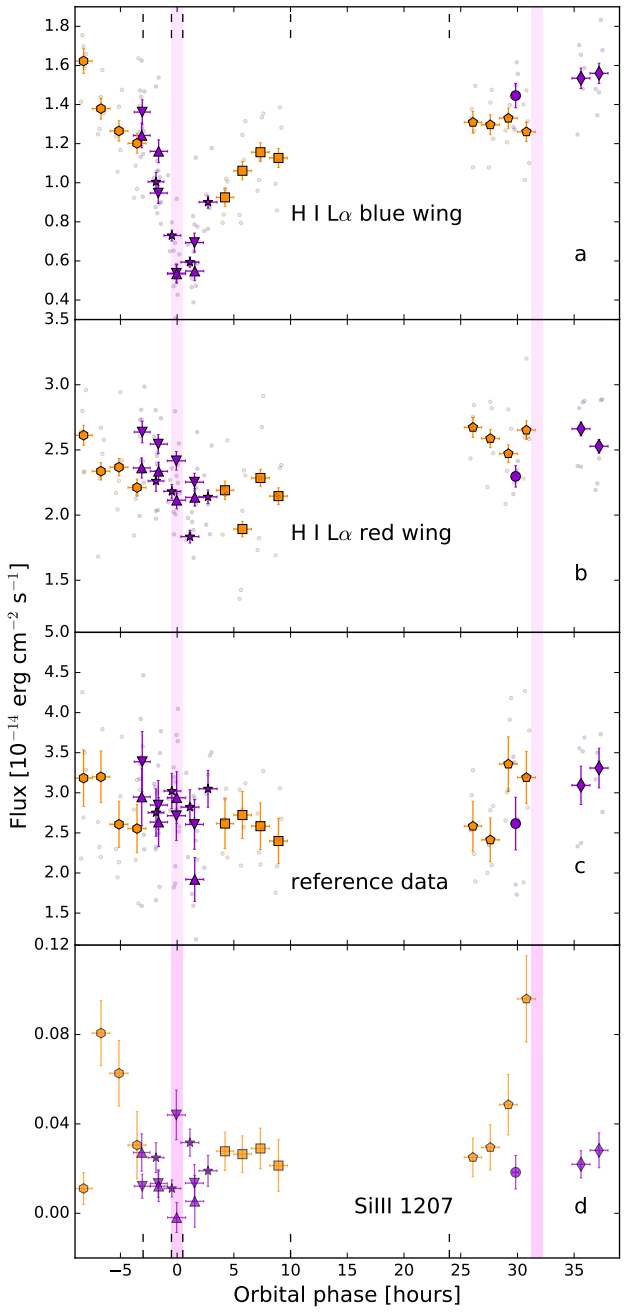

Fig. A.1. Lyα light curve of GJ 436 obtained from integrating the raw spectra uncorrected for systematics. The flux is integrated over the blue wing $[-120, -40]$ km s^{-1} (*a*), the red wing $[+30, +120]$ km s^{-1} (*b*), the reference band $[-250, -120] \cup [+120, +250]$ km s^{-1} (*c*), and the $[-50, 50]$ km s^{-1} band of the Si III line (*d*). The colour code is the same as in Fig. 1. Large coloured symbols with errors bars are the individual HST orbits (see Table A.1 for the visit symbols) while small grey circles are the time-tagged sub-exposures extracted from each HST orbit for *panel a, b*, and *c*.

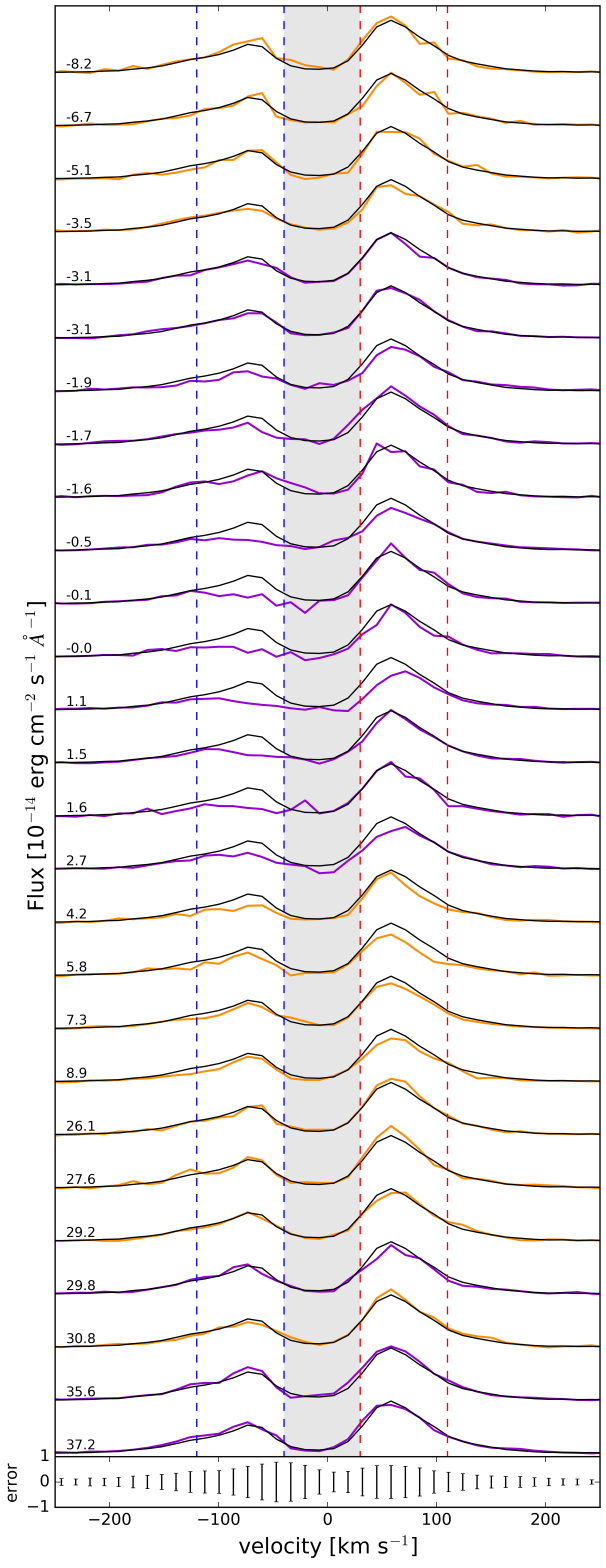

Fig. A.2. New visits described in this work are in orange while previous visits are plotted in violet. Lyα line spectra of GJ 436 of each HST orbit compared to the unocculted line (black curves) obtained by combining all spectra from the out-of-transit phases region (see Sect. 3.3). The number on top of each spectrum indicates the time in hours from the mid-transit time. Vertical dashed lines indicate the blue and the red bands showing absorption signatures. The grey zone is the geocoronal emission (airglow) band.

Table A.1. Observation log.

Visit	Date	Programme	PI	HST orbits	Time from mid-transit (h)	Phase range
0 (○)	01 May 2010	GO#11817	Ehrenreich	1	[29.64, 30.03]	[0.46, 0.47]
1 (★)	07 Dec. 2012	GTO#12034	Green	4	[−2.03, 3.04]	[−0.03, 0.05]
2 (△)	18 Jun. 2013	GO#12965	Ehrenreich	4	[−3.26, 1.75]	[−0.05, 0.03]
3 (▽)	23 Jun. 2014	GO#12965	Ehrenreich	4	[−3.30, 1.78]	[−0.05, 0.03]
4 (⋄)	25 Jun. 2015	GO#13650	France	2	[35.29, 37.49]	[−0.44, −0.41]
5 (⬠)	30 Mar. 2016	GO#14222	Ehrenreich	4	[25.86, 31.04]	[0.40, 0.49]
6 (□)	06 Apr. 2016	GO#14222	Ehrenreich	4	[4.01, 9.18]	[0.06, 0.14]
7 (⬡)	08 May 2016	GO#14222	Ehrenreich	4	[−8.45, −3.28]	[−0.13, −0.05]

Notes. Symbols in the first column refer to plotting symbols in Fig. A.1.

Table A.2. Orbital phases range.

Phase range	HST orbits [visit #, (orbit #)]
Before transit	[2, (1)], [3, (1)], [7, (1, 2, 3, 4)]
Ingress	[1, (1)] , [2, (2)], [3, (2)]
Optical transit	[1, (2)] , [2, (3)], [3, (3)]
Egress	[1,(3, 4)] , [2, (4)], [3, (3)], [6,(1, 2, 3, 4)]
After transit	[0, (1)], [4,(1, 2)], [5, (1, 2, 3, 4)]

Appendix B: Correction of systematics: Gaussian processes

This method differs from the parametric approach in that the shape of the function used to describe the systematics can be adjusted to capture any behaviour not encompassed by an analytical function. Gaussian processes (GP) are one of these methods. GP are widely use in machine learning and are increasingly popular in the exoplanet community (see Williams 2006 for a global introduction and Gibson et al. 2012 for an application in the exoplanet field). Within a GP scheme, the joint probability distribution for the reference band is a multivariate gaussian distributed about a mean function, a flat line representing a stable flux in our case. Systematics and white noise are characterised by the covariance matrix, which is defined by a covariance function (or kernel). In this analysis we adopt the squared exponential kernel in addition to a white kernel: $k(t,t') = \exp(\frac{-\|t'-t\|/^2}{2l^2}) + \delta_{tt'}\sigma^2$. The hyperparameter l of the squared exponential kernel defines a characteristic length scale above which data points are not correlated. The white noise is incorporated through a variance term σ (an hyperparameter) with $\delta_{tt'}$ being the Kronecker function. The white noise should describe the pipeline error bars and the length scale should be of the order of one HST visit duration. Having a shorter length scale can allow us to reproduce shorter features providing a better correction of the systematics. However, it may lead to an over fitting. GP are implemented using George (Ambikasaran et al. 2014).

We note that Visit 0 only has one orbit, which makes the correction of the breathing effect ambiguous as its reproducibility between orbits of the same visit cannot be assessed. Therefore, we did not correct the fluxes from this visit.

Appendix C: Other lines

Apart from the Lα line, we have identified several other lines: Si III at 1206.51 Å, N V at 1238.821, 1242.804 Å, and O V at 1218.344 Å. Those lines have a flux two magnitudes lower than the Lα line. The flux measured during one single orbit is in a photon-starved regime and can present strong variations of magnitude (even a negative flux) and shape from one orbit to another. We therefore averaged all the spectra within the orbital phase regions labelled A to E on Fig. 1 (cf. Table A.2): (A) before the exospheric transit signature in the blue wing of Lyα, (B) during the exospheric transit ingress, (C) during the optical transit, (D) during the exospheric transit egress, and (E) after the exospheric transit. Regions (B), (C), and (D) are considered "in-transit"; regions (A) and (E) are "out of transit". We consider the flux integrated in the velocity band [–50, 50] km s^{-1}. Let $F_{\rm in}$ and $F_{\rm out}$ be those fluxes during the transit and out of the transit respectively (dashed lines in Fig C.2). The absorption is defined as $1 - F_{\rm in}/F_{\rm out}$. Table C.1 shows results for each line. The N V lines are summed together in the velocity space. No absorption is observed for this specie. An absorption signal is measured in the O V line, but it may not be related to the planet as only the ingress

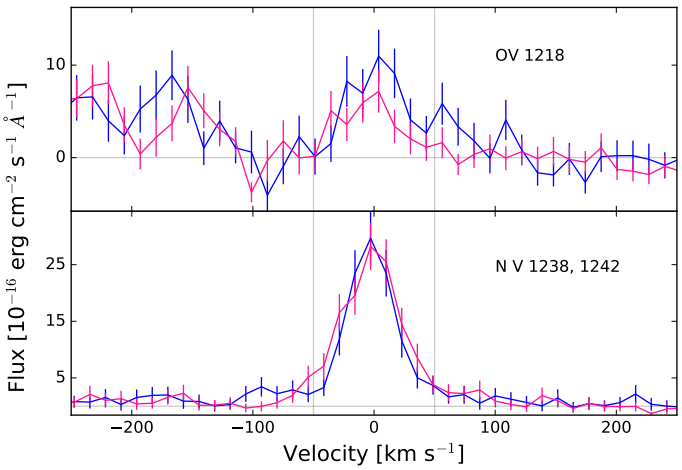

Fig. C.1. Averaged out-of-transit (blue) and in-transit (pink) spectra of the O V at 1218.344 Å (*top panel*) and the N V doublet at 1238.8 Å and 1242.8 Å (*bottom panel*) with both lines summed in velocity space. Vertical grey line indicates the [−50, +50] km s^{-1}area.

Table C.1. Identified stellar lines in STIS/G140M.

Species	Wavelength [Å]	Stellar flux (10^{-16} erg cm^{-2} s^{-1})	Absorption %
Si III	1206.510	3.8 ± 0.3	47 ± 10
O V	1218.344	2.2 ± 0.2	36 ± 15
N V	1238.8 1242.8	5.5 ± 0.3	−0.07 ± 12

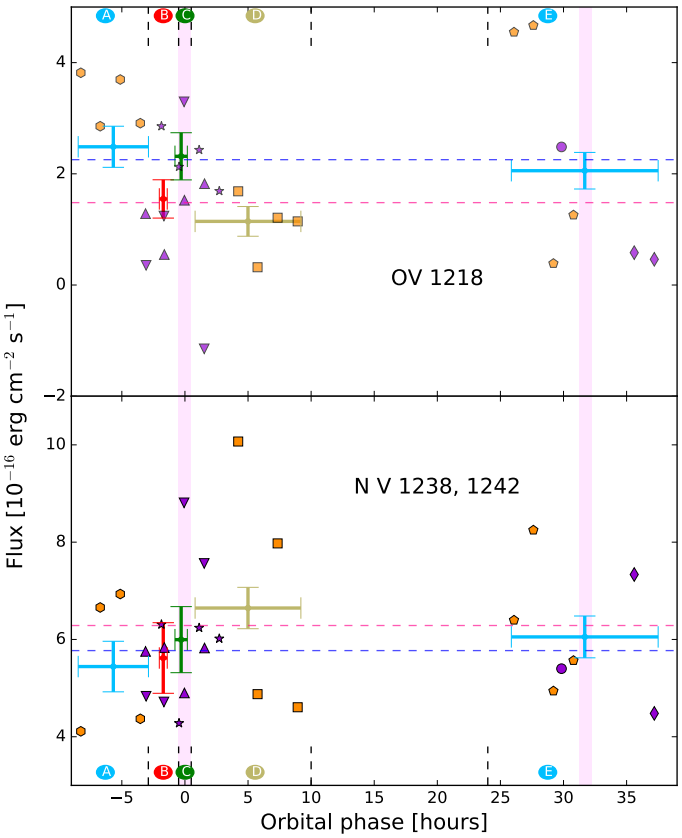

Fig. C.2. Light curves of GJ 436 O V line (*top panel*) and N V (*bottom panel*). Legend is the same as in Fig. 1. Fluxes are integrated for the different temporal regions (see Fig. 1). Horizontal dashed line indicates the out-of-transit flux (blue – regions A and E) and the in-transit flux (pink – regions B, C, and D). Symbols indicate the orbit fluxes (see Table A.1)

and egress fluxes are absorbed. Finally, an absorption signal in Si III line correlated with the planet transit is detected at almost five sigma (see Sect. 4.3).